Plant, Cell and Environment (2008) **31**, 1349–1360 doi: 10.1111/j.1365-3040.2008.01839.x

Drought-induced changes in anthesis-silking interval are related to silk expansion: a spatio-temporal growth analysis in maize plants subjected to soil water deficit

AVAN FUAD-HASSAN, FRANÇOIS TARDIEU & OLIVIER TURC

INRA and Montpellier SupAgro, UMR 759 Laboratoire d'Ecophysiologie des Plantes sous Stress Environnementaux, 2 place Viala, F-34060 Montpellier, France

ABSTRACT

The growth and emergence of maize silks has a considerable importance in yield determination under drought conditions. Spatial and temporal patterns of the rates of tissue expansion and of cell division were characterized in silks of plants subjected to different soil water potentials. In all cases, silk development consisted of four phases: (1) cell division and tissue expansion occurred together uniformly all along the silk; (2) cell division progressively ceased from tip to base, while expansion remained spatially uniform including during the phase (3) after the cessation of cell division; and (4) as the silk emerged from the husks, expansion ceased in the emerged portion, probably because of direct evaporative demand, while the relative growth rate progressively decreased in the enclosed part. The rates of tissue expansion and cell division were reduced with water deficit, resulting in delayed silk emergence. The duration of cell division was not affected, and in all cases, the end of cell division in the silk coincided with anther dehiscence. The duration of phase 3, between the end of cell division and the arrest of cell growth in silk apex, considerably increased with water deficit. It corresponded to the anthesis-silking interval used by breeders to characterize the response of cultivars to stress.

Key-words: maize (*Zea mays* L.); cell division; soil water potential; stigma; tissue expansion.

INTRODUCTION

The growth and emergence of maize silks has a considerable importance in the determination of yield under drought. When soil water deficit occurs before flowering, silk emergence out of the husks is delayed while anthesis is largely unaffected, resulting in an increased anthesis-silking interval (ASI) (Edmeades *et al.* 2000). Selection for reduced ASI has been used successfully to increase the drought tolerance of maize (Edmeades *et al.* 1993; Bolanos & Edmeades 1996; Bruce, Edmeades & Barker 2002). Co-locations of quantitative trait loci (QTLs) for increased grain yield and short ASI under drought conditions (Ribaut *et al.* 1997) indicate that the maintenance of grain yield under water stress is genetically linked to the maintenance of rapid silk growth.

However, silk growth has never been analysed in detail. It is therefore not possible to organize sampling for omics studies based on the temporal or spatial patterns of growth, to the difference of leaves (Vincent *et al.* 2005; Muller *et al.* 2007) or roots (Poroyko *et al.* 2007). Silks are specialized tissues of the female inflorescence that are functionally equivalent to the stigma and style portions of typical pistils (Kroh, Gorissen & Pfahler 1979; Heslop-Harrison, Reger & Heslop-Harrison 1984). Silk development is a long process, lasting several weeks from silk initiation to silk emergence (Ruget & Duburcq 1983; Carcova, Andrieu & Otegui 2003), while senescence occurs a few days after emergence, even in the absence of ovule fertilization (Bassetti & Westgate 1993b; Anderson *et al.* 2004). Spatial analyses of silk growth are scarce, essentially qualitative and somewhat contradictory. According to Kiesselbach (1999), a growth zone where new cells develop is located at the base of the silk and causes continuous elongation. This growth pattern, close to that of monocot leaves, would continue until fertilization, when the zone of new growth shrivels up. Conversely, Westgate & Boyer (1985) showed with ink marks on the silk surface that elongation occurs all along the silk, so the growth zone would not be spatially restricted to the silk base. Epidermal cell lengths measured at different stages of silk growth suggested that cell division in the basal zone stops during early stigma development, and silk elongation is essentially achieved by cell expansion (Heslop-Harrison *et al.* 1984).

Furthermore, the physiological determinants of ASI in terms of growth analysis are unknown, making it difficult the identification of candidate mechanisms for a genetic analysis. The sensitivity of silk growth to soil water deficit has been examined by several authors who measured the growth rate of emerged silks (Herrero & Johnson 1981; Westgate & Boyer 1985; Bassetti & Westgate 1993c). The rate of silk elongation tends to parallel leaf water potential (Herrero & Johnson 1981), which remains close to silk water potential (Westgate & Boyer 1986; Westgate &

Correspondence: O. Turc. Fax: +33 (0)467 522 116; e-mail: turc@supagro.inra.fr

Thomson Grant 1989). However, because ASI is the result of silk growth from initiation to emergence, there is a need for analysing and quantifying the effect of water deficit on silk growth and cell division during this whole period.

The objective of this paper was to identify the temporal and spatial patterns of silk growth and cell division as affected by water deficit. For this purpose, kinematic analyses were carried out from silk initiation to completion of elongation, and involved silks from the fifth spikelet, counted from the ear base, which are the first silks to emerge out of the husks (Bassetti & Westgate 1993a). Plants were either well watered (soil water potential higher than –0.1 MPa), or subjected to a mild (soil water potential between –0.5 and –0.3 MPa) or a medium soil water deficit (between –0.8 and –0.6 MPa).

THEORY

A direct method to analyse the spatial distribution of tissue growth is to follow the displacement with time of tissue particles, identified with ink marks or pin holes distributed on the organ surface. When cells are aligned along files, as it is the case for epidermal cells of maize silks (Fig. 1), counting the number of cells between two marks allows the calculation of the local rate of cell division (Silk 1992; Tardieu & Granier 2000). The length (L_i) of a zone i between two marks is the product of the number of cells (N_i) by the average cell length (λ_i) in the zone i. The local relative segmental growth rate [$r_i = (\Delta L_i/\Delta t)/L_i$] therefore equals the sum of the relative cell division rate [$\eta_i = (\Delta N_i/\Delta t)/N_i$] and the relative cell expansion rate [$c_i = (\Delta\lambda_i/\Delta t)/\lambda_i$]. The local rate of cell division is therefore deduced from direct measurements of local expansion (with marks) and local cell length in the considered zone. In case of steady growth, time courses of the cell division rate, tissue expansion rate and individual cell expansion rate can be inferred from spatial distributions of cell length and tissue expansion (Silk 1992) with a limited number of sampling dates. In the opposite case, the analysis should take into account the changes in distributions of the same variables along the organ during the period of organ development, which requires a large number of sampling dates and spatial analyses. Nevertheless, the analysis can be simplified in two cases.

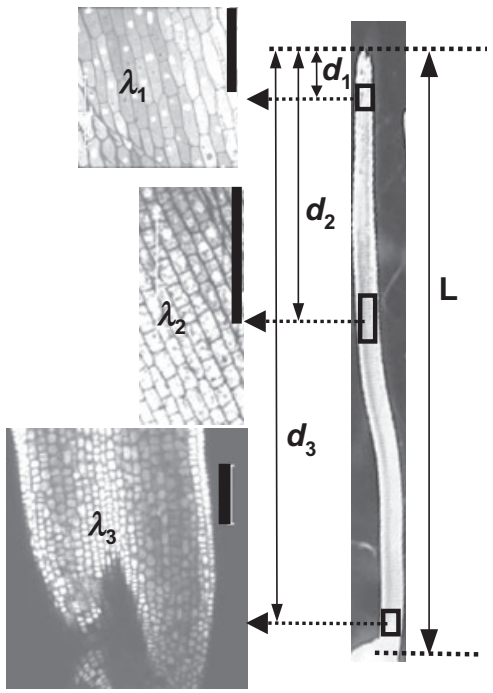

Figure 1. Epidermal cell lengths at different spatial positions along a maize silk. Depending on silk length L, 5–25 microphotographs of silk surface were taken at regular intervals from the apex to the base to visualize epidermal cell files. For clarity, only three measurement points are presented here. For each photograph i, the distance from silk apex d_i [or from silk base $(L - d_i)$] was recorded, and the mean length λ_i of 20–50 cells was measured. Bars, 100 μm.

1 When no cell division occurs in the considered zone of the silk ($\eta_i = 0$), the relative segmental growth rate r_i equals the relative cell expansion rate c_i. The spatial position of the cells located in the ith zone can be characterized by their rank n along the cell files, counted from a fixed reference point. For a given tissue particle, this position mark n is stable with time because of the absence of cell production. In this particular case, the physical marks can be replaced by the limits between cells and r_i deduced from average cell length λ_n in the nth cellular cohort at times t and $t + \Delta t$:

$$r_i = c_i = c_n = (\Delta\lambda_n/\Delta t)/\lambda_n \quad (1)$$

where the ith spatial zone is chosen to be the location of the nth cellular cohort at both dates t and $t + \Delta t$.

2 When the growth rate is uniform along the silk (r_i is position invariant), the relative rate of tissue expansion in each zone equals the relative growth rate of the whole silk:

$$r_i = r = (\Delta L/\Delta t)/L \quad (2)$$

The local rate of cell division η_i is calculated as

$$\eta_i = r_i - c_i = (\Delta L/\Delta t)/L - (\Delta\lambda_i/\Delta t)/\lambda_i \quad (3)$$

The spatial position of a given zone i can be characterized by its distance from a fixed reference point (e.g. silk base) divided by silk length [$(L - d_i)/L$] (Fig. 1). This position mark is conserved with time because all material points move away from the others at the same rate in this particular case.

MATERIAL AND METHODS

Plant culture conditions

Three experiments were carried out in the greenhouse and in the growth chamber in the phenotyping platform Phenodyn (Sadok *et al.* 2007). Three seeds of maize inbred

line F252 (American early dent line) were sown in 72 polyvinyl chloride pots containing 12 L of a mixture of loamy soil (aggregate diameter ranging from 0.1 to 4.0 mm) and organic compost in volumes of 0.4:0.6. The pots were watered daily with a modified tenth-strength Hoagland solution supplemented with minor nutrients.

Air temperature and relative humidity were measured every minute at plant level (HMP35A; Vaisala Oy, Helsinki, Finland). The temperature of the growing ear of 12 plants per experiment was measured with a fine copper-constantan thermocouple (0.2 mm diameter) located inside the ear-leaf sheath or inside the husks when they became visible. Light was measured every minute using two photosynthetic photon flux density (PPFD) sensors (LI-190SB; Li-Cor, Inc., Lincoln, NE, USA). All data of temperature, PPFD and relative humidity were averaged and stored every 15 min in a data logger (LTD-CR10X wiring panel; Campbell Scientific, Leicestershire, UK).

The average temperature in the greenhouse ranged from 16 to 20 °C and from 20 to 25 °C during the night and day, respectively, and the vapour pressure deficit (VPD) never exceeded 1.2 kPa during plant growth. Additional light was provided by a bank of sodium lamps that maintained the PPFD above 200 μmol m^{-2} s^{-1} for 12 h d^{-1}. Plants were transferred just before silk emergence in a growth chamber where stable environmental conditions were maintained until completion of silk growth: 12 h photoperiod; 22/20 °C day/night temperature; VPD, 0.8–1.0 kPa; PPFD, 450–550 μmol m^{-2} s^{-1} at ear-leaf level. Soil water content was determined before sowing to estimate the amount of dry soil and water in each pot. Subsequent changes in pot weight were attributed to changes in soil water status after correction for plant weight (root + shoot fresh weight) measured on frequently harvested plants. This allowed the calculation and adjustment of soil water content to target values corresponding to the desired soil water potential. Until the initiation of the first silks, all pots were watered in order to maintain the soil water content around 0.42 g g^{-1}. From this stage onwards, the pots were distributed in three groups with different levels of soil water content: 0.42 (well watered), 0.24 (mild deficit) and 0.20 g g^{-1} (medium deficit), corresponding to the ranges of water potential from –0.05 to –0.10 MPa in well-watered plants, from –0.3 to –0.5 MPa in mild deficit, and from –0.6 to –0.8 MPa for medium deficit. In the two water deficit treatments, irrigation was withheld until the soil water content reached the target values of the soil water content, which was then maintained stable by controlling daily the pot weight before and after irrigation.

The number of ligulated leaves and of visible leaf tips were recorded every second day on all plants. The dates of visible reproductive stages (tassel emergence, anthesis and silk emergence) were recorded with daily observations of individual plants. Floral development of the uppermost axillary bud was inspected by dissecting the ears of two plants twice a week from six-leaf stage to silk initiation. Stable correspondences between leaf stage and floral development were established for the studied line in our conditions: spikelet initiation began when the number of visible leaf tips reached 0.65 of final leaf number, and the first silk initiation (basal spikelets with a silk of 0.1 mm long) occurred 160 °Cd (15–16 d in our conditions) later. The date of silk initiation, used as time origin in the present study, was therefore estimated for each individual plant. Time was expressed in thermal units (°Cd) taking into account the ear temperature, with a threshold temperature of 9.8 °C (Ben Haj Salah & Tardieu 1996; Carcova *et al.* 2003). Male inflorescences (tassels) were excised just before pollen shedding to avoid an early arrest of silk growth because of ovule fertilization (Kiesselbach 1999).

Growth analysis

Silk length, epidermal cell length and the number of epidermal cells

Two plants per treatment were sampled daily from silk initiation to silk emergence, and every second day later on. At early developmental stages, the ear was dissected under a binocular (Leica MZ75; Leica Microsystems GmbH, Wetzlar, Germany). Husk tissues were gently removed with a fine scalpel blade to allow a clear view of successive flowers along the ear. The lengths of four to six silks, originating from flowers in the fifth position counted from the ear base, were measured with an interactive image analysis system (Optimas 6.5; Media Cybernetics, Inc., Bethesda, MD, USA) coupled to the binocular. The distance L_h between the silk insertion point (fifth flower along the ear row) and the husk tip was measured in the same way. At later stages, the silks were carefully excised and measured with a ruler. One of the measured silks was then transferred in a mixture of ethanol (70% v/v), formaldehyde and acetic acid, and was stored until observations of epidermal cells were made under a microscope (Leica DM 6000 B; Leica Microsystems GmbH). Well-ordered silk segments were slide-mounted, and a series of microphotographs of epidermal cells was carried out at regular intervals from the silk apex to the silk base (5–25 photographs per silk, according to silk length). For clarity, only three photographs are presented in Fig. 1. The spatial position of each photograph [distance from the silk apex d_i or from the silk base $(L - d_i)$] was calculated from the automated recording of coordinates of the observed zone on the microscope stage. The length of epidermal cells (λ_i) was measured (mean of 20–50 cells) with the image analysis system. Between two successive measurement points, the number of cells along the cell file was estimated by linear interpolation as

$$N_i = (d_{i-1} - d_i)/[(\lambda_{i-1} - \lambda_i)/2] \quad (4)$$

The total number N of cells per cell file along the whole silk was obtained by cumulating the values N_i from the silk apex to the base.

$$N = \sum N_i \quad (5)$$

The rank n of the cellular cohort located in the ith spatial zone was calculated as the sum of N_j between the silk apex and the measurement point i.

$$n = \sum N_j (1 \le j \le i) \quad (6)$$

This allowed the calculation of the local growth rates of tissue elements where and when cell division had ceased (Eqn 1).

Local growth rates measured with ink marks

An analysis of ink marks displacement, therefore independent of cell walls, was used in short-term experiments to test the uniformity of elongation along the silks during their early development. Plants were placed in a growth chamber equipped with a system used to guide and visualize a pressure probe inside individual cells (Bouchabke, Tardieu & Simonneau 2006). The husks enclosing the ear were carefully cut and peeled away. Ink marks were deposited with a needle mounted onto a micromanipulator (Leitz mechanical joystick manipulator; Leitz, Jena, Germany) facing to an XY stage where the plant was installed. The precise location of ink deposit was controlled by an orthogonal video microscope system equipped with a zoom (×20 to ×150 monozoom; Leica, Buffalo, NY, USA). Ink marks were placed every 2 mm for the silks around 10–20 mm long, every 5 mm for the silks around 40–50 mm long, and every 10 mm for longer silks, in order to obtain at least six to eight measurement points regularly distributed from the silk apex to the base. The husks were then replaced, and the entire ear was enclosed in a plastic bag lined with wet paper towels. The growth chamber was maintained at 25 °C, near 100% humidity, and dark for 24 h. Marked silks were then excised and observed under a microscope coupled to an image analysis system to precisely determine the distance between marks after 24 h of growth. This procedure was performed only during the first experiment at five occasions during the progression of silk development of well-irrigated plants, because it was time-consuming and delicate because of the fragility of young silk tissues. No reliable measurements were obtained before the silks reached 10 mm.

The local relative growth rates r_i were calculated as the relative increase in distance between consecutive marks during the 24 h period. Values of at least 20 silks were averaged for each spatial position expressed as relative distance from the silk base $[(L - d_i)/L]$.

Calculations and curve fit

Because the time courses of silk length and cell number were reproducible among experiments (Fig. 2a,b), data of the three experiments were analysed as a single set, each point corresponding to a plant at a given age t calculated from silk initiation. The silk relative growth rate r and the local relative rate of cell expansion c_i at a given spatial position i were calculated at any given time t from silk initiation to completion of silk growth as the local slope of the relationship between the logarithm of silk length L (respectively local cell length λ_i) and thermal time t:

$$r = \mathrm{d}(\ln L)/\mathrm{d}t \quad (7)$$
$$c_i = \mathrm{d}(\ln \lambda_i)/\mathrm{d}t$$

Local slopes were calculated by linear regression on all available data during a period of 30 °Cd (ca. 3 d) centred on t. The local relative growth rates (r_i) and the local rates of cell division (η_i) were calculated with Eqns 1–3 and 7.

Several variables (silk length L, cell number per file N, local epidermal cell length λ_i) were fitted to combinations of exponential and linear functions of thermal time (see Appendix). The parameters of the functions were estimated by least squares fitting, using an algorithm of generalized reduced gradient (Marquardt-Levenberg algorithm of software SIGMA PLOT 2001 V7.1; SPSS Science, Chicago, IL, USA). In the text and table, the mean values of parameters are followed by the SEs generated by the software.

RESULTS

Four phases characterized the silk development of well-watered plants

A temporal analysis of silk length and cell number per file is presented in Fig. 2. The cell division rate and tissue expansion rate followed similar patterns. An exponential phase with a constant relative rate was followed by a steep decrease in relative rate in both cases, but the decrease in the expansion rate occurred after that of the cell division rate. This pattern was common to the three experiments and allowed the identification of four reproducible phases of development in the silks of well-watered plants.

1. During the first phase, which lasted 80 °Cd (ca. 8 d), both silk length and cell number had exponential increases, resulting in constant values of both the relative growth rate and the cell division rate in the whole silk. This phase stopped when the cell division rate ceased to be constant (Fig. 2b).
2. During the second phase, which lasted from 80 to 120 °Cd (ca. 4 d), the cell division rate progressively decreased in the whole silk (Fig. 2b). The relative growth rate remained maximum and time invariant during this period (Fig. 2b).
3. The third phase began when cell division completely stopped in the silk, while the relative growth rate was still maximum, at 0.052 °Cd^{-1}. This phase was very short in well-watered plants (ca. 1 d), and would probably not have been identified if water-stressed plants had not been analysed in the same experiments (see further discussion).
4. The fourth phase began when the relative growth rate started to decline, and ended with the cessation of silk elongation.

Silk emergence coincided with the end of the exponential phase of silk growth, while the cessation of division

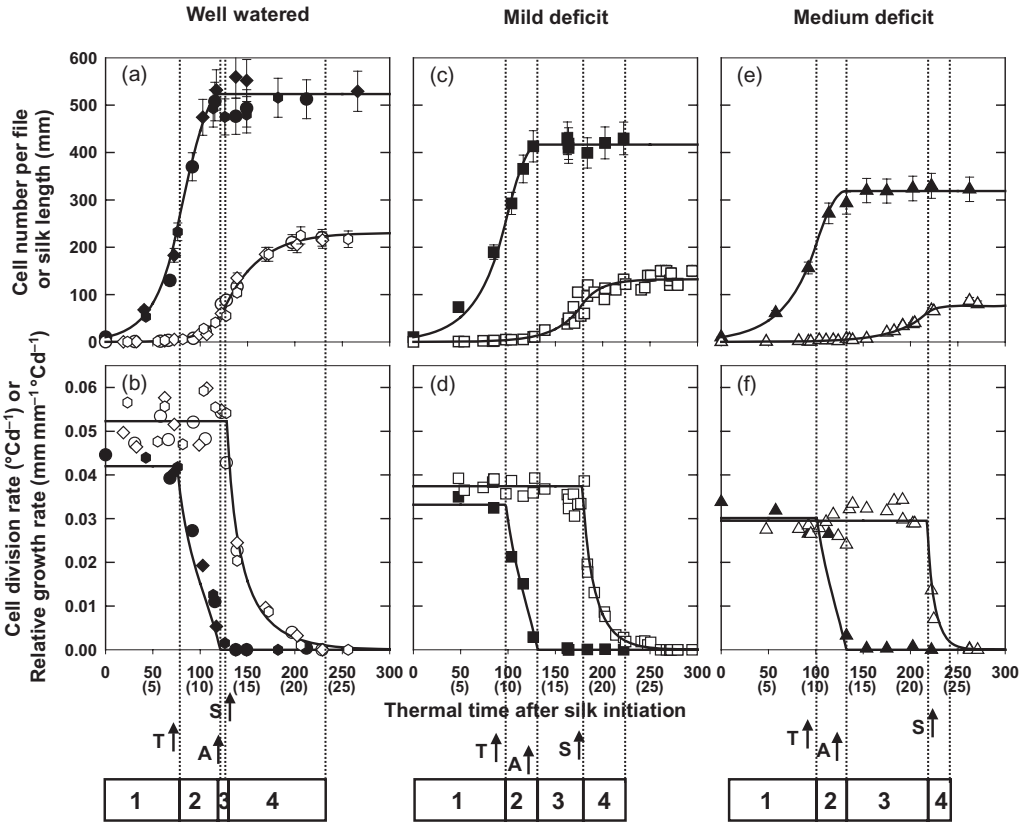

Figure 2. Time courses of cell number per file (closed symbols) and silk length (open symbols) (a, c, e), and of relative rates of cell division (closed symbols) and tissue expansion (open symbols) (b, d, f) as a function of thermal time. Calendar times in days are indicated in parenthesis. Soil water potential was maintained above –0.1 MPa in well-irrigated plants (a, b), between –0.3 and –0.5 MPa for mild deficit (c, d), and between –0.6 and –0.8 MPa for medium deficit (e, f), from silk initiation onwards. Vertical dotted lines indicate the end of each phase of silk development. Solid lines were obtained by fitting data to Eqns 8 and 9. Arrows indicate the dates of occurrence of tassel emergence (T), anthesis (A) and silk emergence (S). Different symbols in (a) and (b) correspond to different experiments.

occurred almost simultaneously with pollen shedding (120 ± 6 and 116 ± 5 °Cd, respectively), so the third phase corresponded to the ASI.

Relative growth rate was spatially uniform during phases 1–3

Experiments with ink marks performed before silk emergence showed that tissue expansion occurred all along the silk, with a uniform relative growth rate from the base to the apex (Fig. 3). Peeling the ears and putting marks on the silk reduced silk growth by 65% (0.052 °Cd^{-1} in Fig. 2 versus 0.018 °Cd^{-1} in Fig. 3), that is, twice the injury effect of pin holes or dissection and ink marks on maize leaf elongation rate (Muller, Reymond & Tardieu 2001). Nevertheless, as commonly accepted for growth spatial analyses in leaves and roots, we assumed that all spatial positions were affected to the same extent, so that the spatial pattern of growth was not modified by injury.

These results indicate that silk growth followed the simple cases described in the theory part, with case 2 occurring during phases 1–3, and case 1 occurring during phases 3 and 4. It was therefore possible to follow the time course

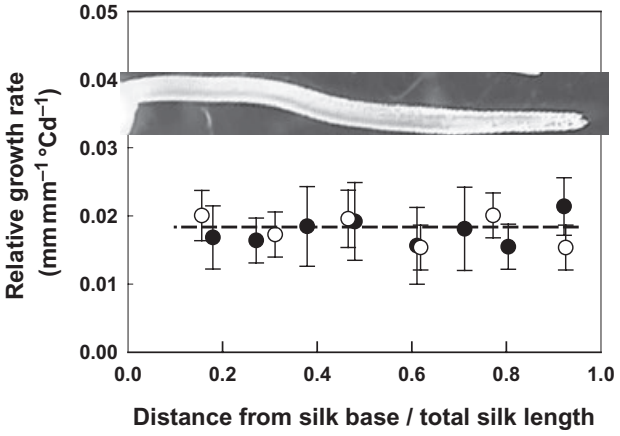

Figure 3. Relative growth rate as a function of the spatial position along the silk. Growth rates were calculated from the displacement of ink marks at silk surface. Data are the means and SEs of measurements carried out on at least 20 silks. Black points correspond to silks marked during phase 1 or 2 (10–20 mm length), and white points to silks marked during phase 3 (30–50 mm length). The spatial position along the silk is expressed as the ratio between the distance from the base ($L - d_i$) and silk length L.

of material points and to calculate the local rates of tissue expansion and cell division without physical marks on the silks (Eqns 1–3).

Spatial and temporal patterns of cell length, tissue expansion and cell division during phases 1–4 of well-watered plants

During phase 1, epidermal cells were short (10–15 μm), without gradient of cell length from the base to the apex (Fig. 4a). The cell division rate was high (ca. 0.04 cell cell^{-1} °Cd^{-1}) and uniform along the silk (Fig. 4b), so the whole silk was meristematic at this stage. Cell length slightly increased with time at all spatial positions because the relative growth rate exceeded the cell division rate (0.050 and 0.041 °Cd^{-1}, respectively). Both the relative rates of cell division and tissue expansion were stable with time in the different zones of the silks (Fig. 5b,c), explaining the exponential increase in silk cell number per file and silk length (Fig. 2). The end of phase 1 corresponded to a reduced cell division rate in the silk tip (Fig. 5b).

During phase 2, cell division stopped very rapidly in the apical part of the silk, while the medium part of the silk had a slower decrease, and the basal part continued dividing at its maximum rate (Fig. 5b). This resulted in a base–tip gradient of the cell division rate at mid-period with, in the basal 10% of the silk, a cell division rate close to the maximum rate observed during the first period (0.041 °Cd^{-1}), and an almost null cell division rate in the apical 10% of the silk (Fig. 4d). The relative growth rate remained maximum and time invariant during this period (Fig. 2c), without an appreciable difference between the apex and the base of the silk (Fig. 3). Because a common relative elemental growth rate involved less cells in the apical than in the basal part of the silk, cell expansion was maximum in the apex and minimum in the base of the silk (Fig. 4d), resulting in an increase in cell length with distance from the base at the end of period 2 (Fig. 4c). This phase therefore corresponded to the rapid decrease until zero of the rates of cell division, successively in the different zones from the silk tip to the silk base (Fig. 5b), while silk growth continued to be exponential (Fig. 5c).

During phase 3, because cell division had ceased, the cell expansion rate equalled the tissue expansion rate without gradient from the base to the tip of the silk (Fig. 4f), thereby confirming the uniform pattern of growth observed with ink marks (Fig. 3). Cell length increased in the whole silk at the same relative rate, and the base–apex gradient of cell length

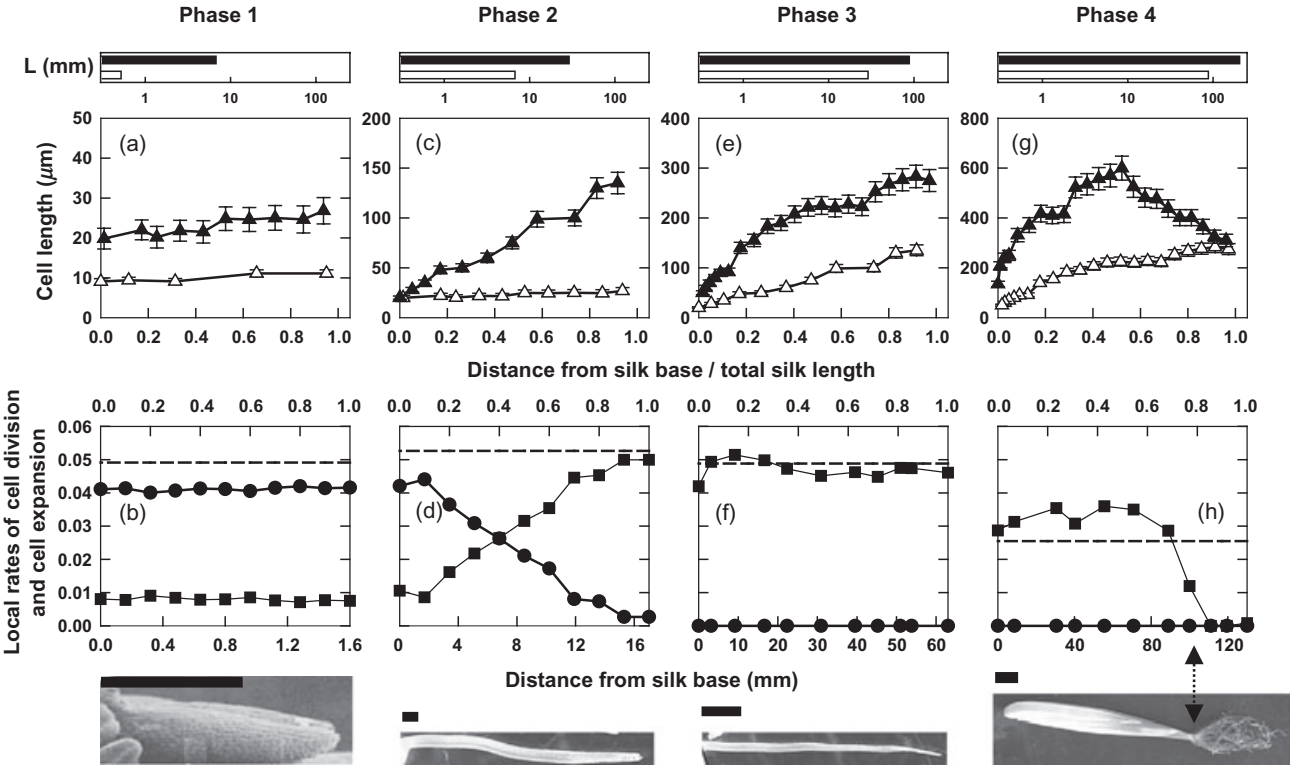

Figure 4. Spatial distribution of cell division and cell expansion during the four phases of silk development. (a, c, e, g) Cell length distribution at the beginning (open triangles) and at the end (closed triangles) of each phase; (b, d, f, h) relative rates of cell division (circles) and cell expansion (squares), calculated at midtime of each phase. Dashed lines indicate the mean relative growth rate of the whole silk. Spatial distributions are plotted against relative position (distance from the silk base divided by silk length). Absolute silk lengths L are given in upper bar charts, at the beginning (white bars) and at the end (black bars) of each phase. Distances on bottom x-axis and photographs correspond to representative silks harvested at midtime of each phase. Scale bars: 1 mm for phases 1 and 2; 10 mm elsewhere.

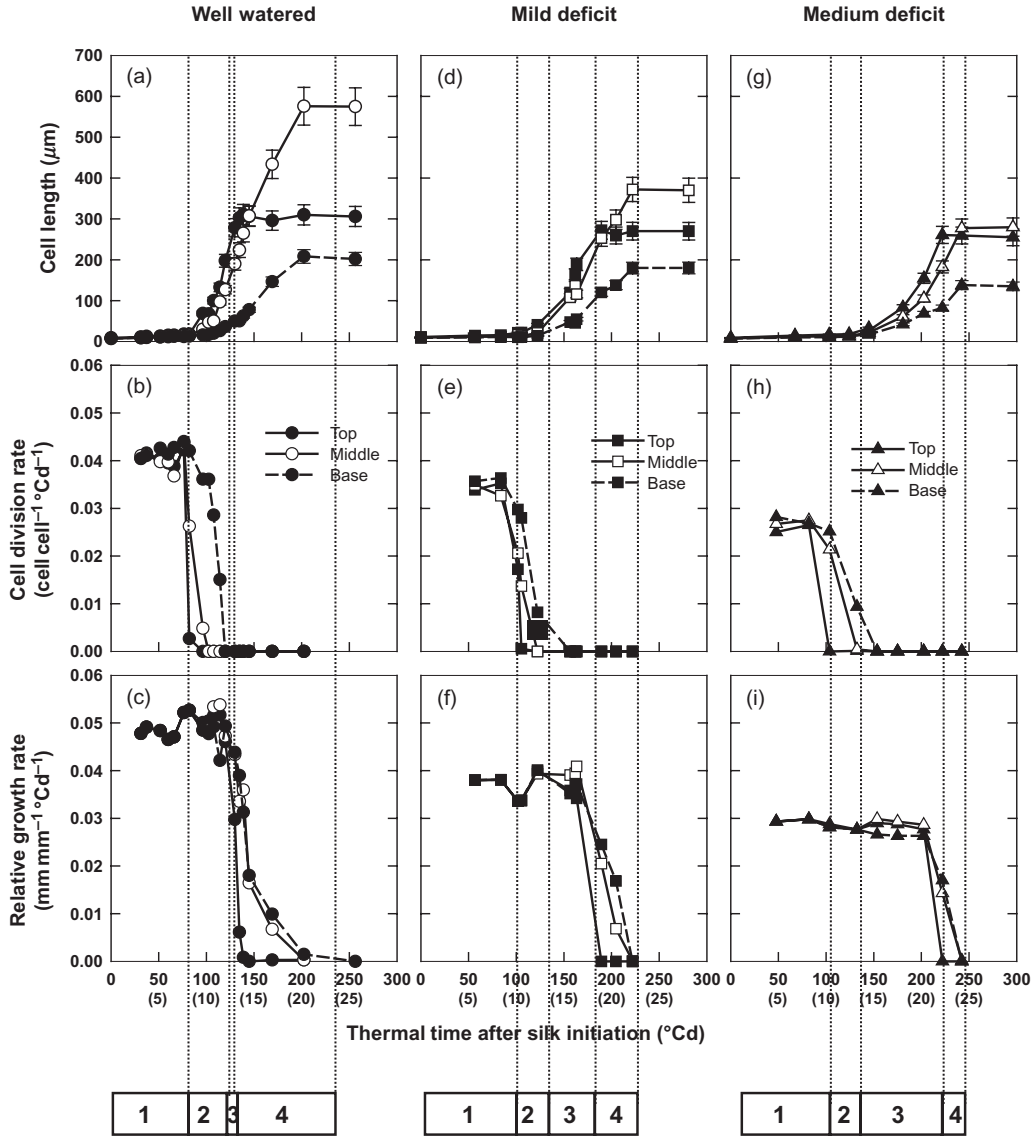

Figure 5. Time course of epidermal cell length (a, d, g), relative rate of cell division (b, e, h) and relative growth rate (c, f, i) in three silk zones (top, middle and base) of plants subjected to different soil water potentials from silk initiation onwards. Calendar times in days are indicated in parenthesis. Soil water potential was maintained above –0.1 MPa in well-irrigated plants (a–c), between –0.3 and –0.5 MPa for mild deficit (d–f), and between –0.6 and –0.8 MPa for medium deficit (g–i). Vertical dotted lines indicate the end of each phase of silk development.

increased with time (in absolute values) between the beginning and the end of period 3 (Fig. 4e).

The decline in the relative growth rate at the beginning of the fourth phase (Fig. 2b) was due to two causes. Firstly, the emerged parts of the silk rapidly stopped elongating (Figs 4h & 5c), thereby causing a non-exponential growth at the whole silk level because the growth rate was not proportional to silk length anymore. We checked with ink marks that the emerged part of the silk did not elongate, regardless of the silk age (data not shown). The second cause was that the relative growth rate declined even in the non-emerged parts of the silks (Fig. 5c), but without gradient between the base and the apical non-emerged zones (Fig. 4h). The cessation of elongation occurred first at the silk apex, and progressed basipetally along the newly emerged silk tissues. As a consequence, the basal and medium parts of the silk grew for a longer duration than the apical part (Fig. 5c). An apex–base gradient of cell length was therefore superimposed on the base–apex gradient observed in phases 2 and 3, resulting in a maximum cell length in the middle of the silk at the end of period 4 (Fig. 4g).

The same model of silk development applied to well-irrigated and water-stressed plants

The same successive phases of development were observed in well-watered plants and in the two water deficit

	Well watered	Mild deficit	Medium deficit
Final silk length (mm)	234 ± 9	132 ± 8	77 ± 4
Final cell number per file	513 ± 17	416 ± 14	319 ± 7
r (10^{-3} mm mm^{-1} °Cd^{-1})	52.4 ± 0.4	37.6 ± 0.4	29.5 ± 0.3
η (10^{-3} cell cell^{-1} °Cd^{-1})	40.7 ± 1.0	33.1 ± 0.7	29.8 ± 0.8
End of phase 1	79 ± 5 (7.7)	98 ± 7 (9.6)	102 ± 10 (10.0)
End of phase 2	120 ± 6 (11.8)	131 ± 7 (12.8)	133 ± 9 (13.0)
End of phase 3	126 ± 3 (12.4)	179 ± 7 (17.5)	218 ± 6 (21.4)
End of phase 4	234 ± 5 (22.9)	221 ± 6 (21.7)	229 ± 10 (22.5)
Tassel emergence	71 ± 5 (7.0)	86 ± 6 (8.4)	91 ± 6 (8.9)
Pollen shedding	116 ± 5 (11.4)	117 ± 6 (11.5)	121 ± 5 (11.9)
Silk emergence	133 ± 6 (13.0)	174 ± 7 (17.1)	224 ± 10 (22.0)

Table 1. Final values and growth parameters of silk length and silk cell number per file during the four phases of silk development

Dates of reproductive stages are also indicated to show synchronisms with silk growth phases. η and r are the rates of cell division and tissue expansion during exponential phases. Soil water potential was maintained above –0.1 MPa in well-irrigated plants, between –0.3 and –0.5 MPa for mild deficit, and between –0.6 and –0.8 MPa for medium deficit, from silk initiation onwards. Dates are expressed in thermal time (°Cd) after silk initiation (mean values ± SE). Calendar times expressed in days, corresponding to daily average temperature of 20 °C, are indicated in parenthesis.

treatments (Fig. 2). In particular, the changes with time in spatial distributions of cell division and tissue expansion described for well-watered plants were also observed in the silks of plants subjected to mild (Fig. 5d–f) or medium (Fig. 5g–i) soil water deficits. The cell division and tissue expansion rates were affected during the whole phase 1, with a common reduction throughout the silk (Figs 2 & 5). As a consequence, no gradient of rates were observed during this phase. The progression of the cessation of cell division and tissue expansion occurred with a base–tip gradient, as in well-watered plants. As a consequence, rapid decreases in the relative rates of expansion and division progressed from the silk apex to the silk base (phases 2 and 4 for the cell division rates and tissue expansion rates, respectively).

Based on these common features in all treatments, we established a set of equations to account for cell division and tissue expansion in growing silks (see Appendix). For each treatment, five parameters – namely the rates of cell division (η) and tissue expansion (r) during exponential phase, the time of cessation of cell division at the silk apex (t_d), and two coefficients characterizing the progressive decrease in the rates of cell division (a_d) and tissue expansion (a_e) – were estimated by fitting equations to the measurements of silk length and cell number per file (solid lines in Fig. 2). The rates, durations, final silk lengths and cell numbers resulting from these calculations are presented in Table 1.

In order to test the consistency of the model, we used the same five parameters – estimated with whole-silk data (cell number, silk length, Fig. 2) – to simulate the time course of individual cell length at any spatial position for the three treatments. The equations presented in the Appendix accounted well for the spatial distribution of cell length for the three treatments as illustrated in Fig. 6 at the four critical dates of silk development (end of uniform cell division rate, end of cell division, silk emergence and end of silk growth).

Soil water deficits imposed from silk initiation onwards reduced both cell number and final silk length with an extent depending on the level of water deficit (Fig. 2 & Table 1). The reduction in cell number was about 20% for a mild deficit, and 39% for a medium deficit. Silk length in the same plants was reduced by 40 and 66%, respectively. This was due to changes in the rates of cell division and tissue expansion, and in the durations of the phases described earlier. During exponential phases, the relative rates of cell division and tissue expansion were reduced by 21 and 29%, respectively, in plants subjected to mild soil water deficit, and by 28 and 44% in plants subjected to medium soil water deficit (Table 1). Cells were shorter in stressed than in well-watered plants (Fig. 6) because the tissue expansion rate was more affected by water deficit than the cell division rate (Fig. 2).

Total durations of cell division and silk growth did not change with water deficit, while phase 3, corresponding to the ASI, was considerably lengthened

The total durations of the periods of cell division (phases 1 + 2) and silk growth (phases 1–4) were not significantly changed by soil water depletion: 120–130 °Cd or 12–13 d for cell division, and 220–230 °Cd or 22–23 d for silk growth (Table 1). Conversely, the durations of the exponential phases (phase 1 for cell division, and phases 1–3 for tissue expansion) increased when soil water potential decreased. The duration of phase 1, from silk initiation to cessation of cell division at the silk apex, increased by 20–25 °Cd (ca. 2 d) in response to drought. The third phase, from the end of cell division to the silk apex emergence, was the most responsive to changes in soil water potential: its end occurred 126 ± 3 °Cd (12.4 d) after silk initiation in well-watered plants, 179 ± 7 °Cd (17.5 d) in plants subjected to

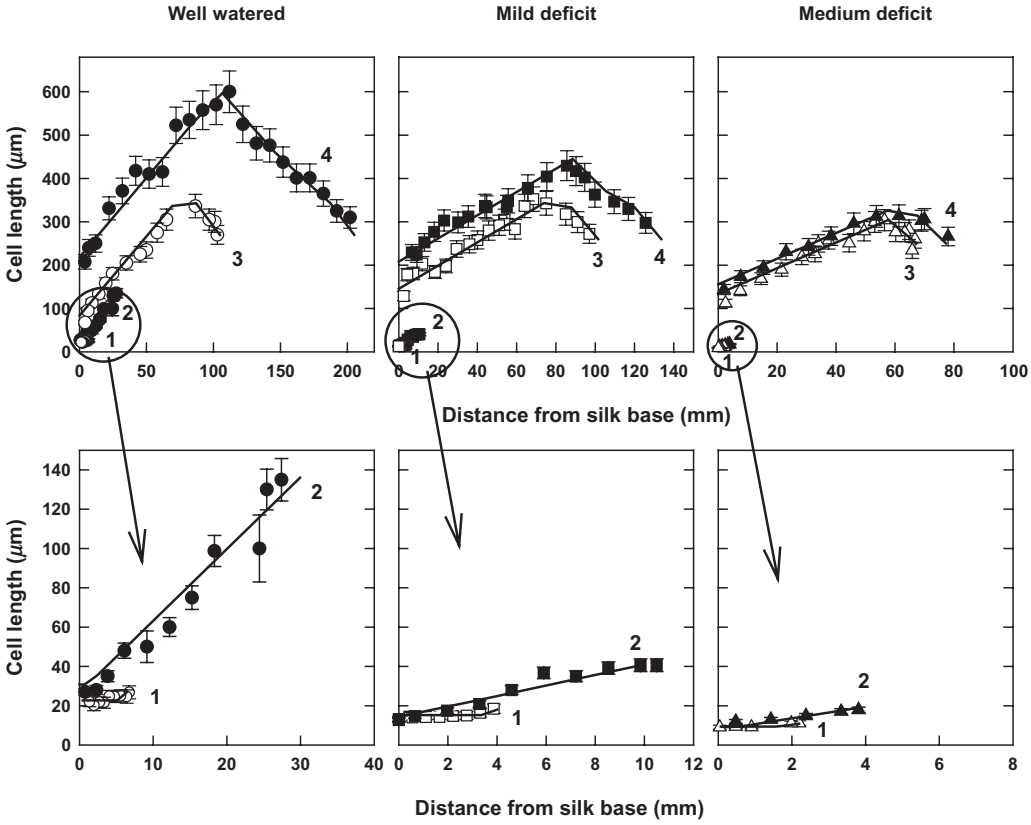

Figure 6. Spatial distribution of epidermal cell length at four critical stages of silk development: 1, end of uniform cell division rate; 2, end of cell division; 3, silk emergence; and 4, end of silk growth. Spatial distributions are plotted against absolute distance from the silk base, with a zoom (lower graphs) to visualize early stages 1 and 2. Soil water potential was maintained above –0.1 MPa in well-irrigated plants, between –0.3 and –0.5 MPa for mild deficit, and between –0.6 and –0.8 MPa for medium deficit. Symbols correspond to measurements, and lines to calculations with Eqns 10–12 (Appendix).

mild water deficit, and 218 ± 6 °Cd (21.4 d) in plants subjected to medium water deficit (Table 1).

Silk development was compared with tassel developmental stages in the three treatments. Tassel emergence occurred 71 ± 5 °Cd (7 d) after silk initiation in well-irrigated plants and was slightly delayed by soil water depletion (ca. 20 °Cd or 2 d). It was nearly synchronous (1 d earlier) with the end of phase 1 of silk development in the three cases (Table 1). Pollen shedding was not affected by decreasing soil water potential and occurred about 120 °Cd (12 d) after silk initiation in the three treatments and coincided with, or just preceded, the end of cell divisions in the silk. The third phase of silk development therefore corresponded to the ASI in all three water treatments.

DISCUSSION

Original distribution of local rates of cell division and tissue expansion

This work is, to our knowledge, the first kinematic analysis of silk growth carried out for the whole silk development period and over its whole length. The silks represent a new case of growth pattern. In spite of common morphological features with roots or monocot leaves (longitudinal growth, cell files), neither growth nor cell division was restricted to the base of the silk as they are in a root or in a monocot leaf. Indeed, the spatial distributions of cell division and tissue expansion showed similarities with those observed in leaves of several dicot species (Maksymowych 1973; Granier & Tardieu 1998), where cell division and tissue expansion occur simultaneously in all parts of the growing organ, with age-dependent spatial distributions. Both processes followed a similar pattern, with an exponential phase followed by a steep decrease in relative rate. An increasing tip–base gradient, corresponding to the progressive arrest from the silk apex to the silk base, was observed for both rates, but occurred later for expansion than for cell division. This pattern defined four developmental phases similar to those described in sunflower leaves (Granier & Tardieu 1998), with a period of cell division that represented more than half of the duration from silk initiation to cessation of growth. The pattern of silk growth presented here will help in the design of tissue samplings for quantifications of metabolite, transcripts or proteins (Granier, Inze & Tardieu 2000; Muller *et al.* 2007). Such analyses on silk tissues should either consider the whole silk during phases 1 and 3, or take into account a base–tip gradient during phases 2 and 4.

Growth arrest in the emerged silk tissues is probably due to the increase in evaporative demand because of air exposure

The silk part emerged from the husks never elongated in any of our experiments, regardless of plant water status. This was probably a direct effect of the exposure of silk tissues to evaporative demand in the air. Silk epidermis does not comprise stomata, but transpiration occurs through the discontinuous cuticle of trichomes (Anderson *et al.* 2004). Air evaporative demand exerting on the emerged silk tissues caused a transpiration stream that decreased water potential. Because silk has a low capacity for osmotic adjustment (Westgate & Boyer 1985; Schoper *et al.* 1987), this probably decreased the turgor below the threshold turgor for growth. In this hypothesis, pollen tube penetration (Heslop-Harrison *et al.* 1984) and growth arrest in the exposed tissues both depend on trichome cuticle discontinuities. This system could ensure the co-ordination between the functions of style and stigma. The style function (tissue expansion to ensure access to pollen) is assigned to the enclosed part of the silk, and the stigma function (pollen receptivity and germination) to the exposed tissues, where elongation is no more necessary for pollen accessibility.

Differential responses of cell division and tissue expansion to soil water deficit and consequences on silk receptivity to pollen

Soil water deficit affected cell division and tissue expansion uniformly along the silk. As a consequence, the four-phase pattern of development described for well-irrigated plants was applied to those under water deficit. Soil water depletion reduced the silk growth rate and increased the duration of growth, but the latter did not fully compensate for the former. Because cell division was less affected than tissue expansion by soil water depletion, the lower the soil water potential, the shorter the epidermal cells at the end of the period of cell division. These responses may contribute to maintain silk receptivity to pollen in drought conditions. Trichomes arise from single cells of silk epidermis, and their fate is determined very early. Cuticle discontinuities appear when future trichome cells are not distinguishable from neighbouring epidermal cells (Heslop-Harrison *et al.* 1984) during the period of epidermal cell divisions. As a consequence, the determinism of trichome number and potential silk receptivity is associated with the period of cell division. Interestingly, we observed a synchronism between the stages of male inflorescence development, which determine pollen availability, and those of cell division in silks, which determine potential silk receptivity to pollen. This synchronism was conserved when water availability changed. The partial maintenance of the cell division rates under water deficit is a way to maintain the potential silk receptivity via an adequate number of trichomes. Furthermore, a reduced size of the neighbour epidermal cells increases the density of trichomes per millimeter of exposed silk.

ASI is directly related to processes of tissue expansion

The ASI is a good predictor of grain yield under stress (Edmeades *et al.* 2000). This was explained by considering ASI as a symptom of assimilate partitioning to the developing spikelets (Edmeades *et al.* 1993, 2000). The present work shows that the ASI is directly related to the processes of cell expansion in the silks, and corresponds to the duration between the end of cell division in the silk and the cessation of elongation in the silk apex. In a recent study, common genetic determinisms were found between leaf elongation rate and ASI in response to soil and air water deficit (co-location of six QTLs) in a population of inbred lines from tropical parental lines known for segregating for ASI (Welcker *et al.* 2007). Taken together, these results support the hypothesis that drought tolerance in maize could partly rely on the maintenance of processes of tissue expansion in both vegetative and reproductive organs.

ACKNOWLEDGMENTS

This work was supported by the Generation Challenge Programme and by the French Agence Nationale de la Recherche (Genoplante Waterless project). Avan Fuad-Hassan thanks the French Ministry of Foreign Affairs and the Kurdish Institute of Paris for grants supporting her PhD thesis in France. We thank Jean-Jacques Thioux and Benoît Suard for technical help during the experiments, Johann Dourguia for cell length measurements, and Geneviève Conejero and Jean-Luc Verdeil for access to microscope facilities at the Plateau d'Histocytologie et Imagerie Cellulaire Végétale (Montpellier RIO Imaging).

REFERENCES

Anderson S.R., Lauer M.J., Schoper J.B. & Shibles R.M. (2004) Pollination timing effects on kernel set and silk receptivity in four maize hybrids. *Crop Science* **44,** 464–473.

Bassetti P. & Westgate M.E. (1993a) Emergence, elongation, and senescence of maize silks. *Crop Science* **33,** 271–275.

Bassetti P. & Westgate M.E. (1993b) Senescence and receptivity of maize silks. *Crop Science* **33,** 275–278.

Bassetti P. & Westgate M.E. (1993c) Water deficit affects receptivity of maize silks. *Crop Science* **33,** 279–282.

Ben Haj Salah H. & Tardieu F. (1996) Quantitative analysis of the combined effects of temperature, evaporative demand and light on leaf elongation rate in well-watered field and laboratory-grown maize plants. *Journal of Experimental Botany* **47,** 1689–1698.

Bolanos J. & Edmeades G.O. (1996) The importance of the anthesis-silking interval in breeding for drought tolerance in tropical maize. *Field Crops Research* **48,** 65–80.

Bouchabke O., Tardieu F. & Simonneau T. (2006) Leaf growth and turgor in growing cells of maize (Zea mays L.) respond to evaporative demand under moderate irrigation but not in water-saturated soil. *Plant, Cell & Environment* **29,** 1138–1148.

Bruce W.B., Edmeades G.O. & Barker T.C. (2002) Molecular and physiological approaches to maize improvement for drought tolerance. *Journal of Experimental Botany* **53,** 13–25.

Carcova J., Andrieu B. & Otegui M.E. (2003) Silk elongation in

maize: relationship with flower development and pollination. *Crop Science* **43,** 914–920.
Dosio G.A.A., Rey H., Lecoeur J., Izquierdo N.G., Aguirrezabal L.A.N., Tardieu F. & Turc O. (2003) A whole-plant analysis of the dynamics of expansion of individual leaves of two sunflower hybrids. *Journal of Experimental Botany* **54,** 2541–2552.
Edmeades G.O., Bolanos J., Hernandez M. & Bello S. (1993) Causes for silk delay in a lowland tropical maize population. *Crop Science* **33,** 1029–1035.
Edmeades G.O., Bolanos J., Elings A., Ribaut J.M., Banziger M. & Westgate M.E. (2000) The role and regulation of the anthesis-silking interval in maize. In *Physiology and Modeling Kernel Set in Maizepp* (eds M.E. Westgate & K. Boote), pp. 43–73. Crop Science Society of America, Madison, WI, USA.
Granier C. & Tardieu F. (1998) Spatial and temporal analyses of expansion and cell cycle in sunflower leaves – a common pattern of development for all zones of a leaf and different leaves of a plant. *Plant Physiology* **116,** 991–1001.
Granier C., Inze D. & Tardieu F. (2000) Spatial distribution of cell division rate can be deduced from that of p34 (cdc2) kinase activity in maize leaves grown at contrasting temperatures and soil water conditions. *Plant Physiology* **124,** 1393–1402.
Herrero M.P. & Johnson R.R. (1981) Drought stress and its effects on maize reproductive systems. *Crop Science* **21,** 105–110.
Heslop-Harrison Y., Reger B.J. & Heslop-Harrison J. (1984) The pollen-stigma interaction in the grasses. 5. Tissue organization and cytochemistry of the stigma ('silk') of Zea mays L. *Acta Botanica Neerlandica* **33,** 81–99.
Kiesselbach T.A. (1999) *The Structure and Reproduction of Corn. 50th Anniversary Edition*. Cold Spring Harbor Laboratory Press, New York, NY, USA.
Kroh M., Gorissen M.H. & Pfahler P.L. (1979) Ultrastructural studies on styles and pollen tubes of Zea mays L. General survey on pollen tube growth in vivo. *Acta Botanica Neerlandica* **28,** 513–518.
Maksymowych R. (1973) *Analysis of Leaf Development*. Cambridge University Press, Cambridge, UK.
Muller B., Reymond M. & Tardieu F. (2001) The elongation rate at the base of a maize leaf shows an invariant pattern during both the steady-state elongation and the establishment of the elongation zone. *Journal of Experimental Botany* **52,** 1259–1268.
Muller B., Bourdais G., Reidy B., Bencivenni C., Massonneau A., Condamine P., Rolland G., Conejero G., Rogowsky P. & Tardieu F. (2007) Association of specific expansions with growth in maize leaves is maintained under environmental, genetic, and developmental sources of variation. *Plant Physiology* **143,** 278–290.
Poroyko V., Spollen W., Hejlek L., Hernandez A., LeNoble M., Davis G., Nguyen H., Springer G., Sharp R. & Bohnert H. (2007) Comparing regional transcript profiles from maize primary roots under well-watered and low water potential conditions. *Journal of Experimental Botany* **58,** 279–289.
Ribaut J.M., Jiang C., Gonzalez-de-Leon D., Edmeades G.O. & Hoisington D.A. (1997) Identification of quantitative trait loci under drought conditions in tropical maize. 2. Yield components and marker-assisted selection strategies. *Theoretical and Applied Genetics* **94,** 887–896.
Ruget F. & Duburcq J.B. (1983) Développement reproducteur des bourgeons axillaires chez le maïs: stades de différenciation, nombre de fleurs. *Agronomie* **3,** 797–807.
Sadok W., Naudin P., Boussuge B., Muller B., Welcker C. & Tardieu F. (2007) Leaf growth rate per unit thermal time follows QTL-dependent daily patterns in hundreds of maize lines under naturally fluctuating conditions. *Plant, Cell & Environment* **30,** 135–146.
Schoper J.B., Lambert R.J., Vasilas B.L. & Westgate M.E. (1987) Plant factors controlling seed set in maize. The influence of silk, pollen, and ear-leaf water status and tassel heat treatment at pollination. *Plant Physiology* **83,** 121–125.
Silk W.K. (1992) Steady form from changing cells. *International Journal of Plant Sciences* **153,** S49–S58.
Tardieu F. & Granier C. (2000) Quantitative analysis of cell division in leaves: methods, developmental patterns and effects of environmental conditions. *Plant Molecular Biology* **43,** 555–567.
Vincent D., Lapierre C., Pollet B., Cornic G., Negroni L. & Zivy M. (2005) Water deficits affect caffeate O-methyltransferase, lignification, and related enzymes in maize leaves. A proteomic investigation. *Plant Physiology* **137,** 949–960.
Welcker C., Boussuge B., Bencivenni C., Ribaut J.M. & Tardieu F. (2007) Are source and sink strengths genetically linked in maize plants subjected to water deficit? A QTL study of the responses of leaf growth and of Anthesis-Silking Interval to water deficit. *Journal of Experimental Botany* **58,** 339–349.
Westgate M.E. & Boyer J.S. (1985) Osmotic adjustment and the inhibition of leaf, root, stem and silk growth at low water potentials in maize. *Planta* **164,** 540–549.
Westgate M.E. & Boyer J.S. (1986) Silk and pollen water potentials in maize. *Crop Science* **26,** 947–951.
Westgate M.E. & Thomson Grant D.L. (1989) Water deficits and reproduction in maize. Response of the reproductive tissue to water deficits at anthesis and mid-grain fill. *Plant Physiology* **91,** 862–867.

Received 1 February 2008; received in revised form 28 May 2008; accepted for publication 29 May 2008

APPENDIX

Model description

Cell number

Cell division uniformly occurred all along the silk at a stable rate η until a date t_d, after which it progressively stopped from the silk apex to the silk base (Fig. 5b, e, h). We supposed that the number N_f of cells that have finished to divide increased linearly with time as a proportion a_d of the number of cells per file at t_d (N_d), and that the remaining basal cells ($N - N_f$) continued to divide at the same rate η. Cell division ceased at time t_{end} when N_f equalled N.

$$\begin{aligned}
&0 \le t \le t_d && N = N_0 \times \exp(\eta \times t) \\
&t_d \le t \le t_{end} && dN/dt = (N - N_f) \times \eta \\
& && dN/dt = [N - a_d \times N_d \times (t - t_d)] \times \eta \\
& && N = N_d \times \{a_d \times (t - t_d) + a_d/\eta + (a_d/\eta - 1) \times \exp[\eta \times (t - t_d)]\} \\
& && t_{end} = t_d + \ln[a_d/(a_d - \eta)]/\eta \\
&t > t_{end} && N = N_d \times a_d/\eta \times \ln[a_d/(a_d - \eta)]
\end{aligned} \quad (8)$$

Silk length

Tissue relative growth rate remained stable (r) and spatially uniform during most of silk development until a date t_e, coinciding with silk emergence out of the husks, after which it rapidly decreased (Fig. 5c, f, i). We described this attenuation with the same negative exponential formalism as formerly used for late growth of sunflower leaves (Dosio *et al.* 2003). After t_e, growth was restricted to the silk zone

enclosed in the husks, which length equals the distance L_h between the silk base and the husk tip. L_h was fitted to an exponential function of thermal time t, and parameters were estimated for each treatment (data not shown). t_e was calculated as the time when silk length L equalled L_h.

$$\begin{aligned} t \le t_e \quad & L = L_0 \times \exp(r \times t) \\ t > t_e \quad & dL/dt = L_h \times r \times \exp[-a_e \times (t - t_e)] \\ & L_h = L_{h0} \times \exp(r_h \times t) \\ & L = L_0 \times \exp(r \times t_e) \times \{1 + r/(a_e - r_h) - r \times \\ & \exp[(r_h - a_e) \times (t - t_e)]/(a_e - r_h)\} \end{aligned} \tag{9}$$

Time course and spatial distribution of cell length

The spatial position of the nth cellular cohort, located at the ith spatial zone, was given by its distance d_i from the silk apex, which equals the sum of lengths of more apical cells.

$$d_i = \sum \lambda_j (1 \le j \le n) \tag{10}$$

For each given position i, the critical dates for cell expansion were t_{di} and t_{ei}, respectively, the dates of cessation of division and of emergence out of the husks of the cells at position i, and t_e, the date of silk tip emergence. t_{di} was calculated with Eqn 8 as the time when N_f equalled n:

$$t_{di} = t_d + n/(a_d \times N_d) \tag{11}$$

and t_{ei} as the time when the distance to the silk base ($L - d_i$) equalled L_h. t_{ei} only occurs for the emerged silk parts.

Before t_{di}, the local relative rate of cell expansion c_i equalled the difference $(r - \eta)$ between the relative rates of tissue expansion and cell division. From t_{di} to t_e, it equalled r, then decreased according to Eqn 9, and eventually reached zero at t_{ei} if the position i emerged from the husks.

$$\begin{aligned} 0 \le t \le t_{di} \quad & \lambda_i = \lambda_0 \times \exp[(r - \eta) \times t] \\ t_{di} \le t \le t_e \quad & \lambda_i = \lambda_i(t_{di}) \times \exp[r \times (t - t_{di})] = \lambda_0 \times \\ & \exp[(r - \eta) \times t_{di}] \times \exp[r \times (t - t_{di})] \\ t_e \le t \le t_{ei} \quad & \lambda_i = \lambda_i(t_e) \times \exp\{[1 - \exp(-a_e \times (t - t_e))] \times r/a_e\} \\ t > t_{ei} \quad & \lambda_i = \lambda_i(t_{ei}) \end{aligned} \tag{12}$$